Effect of Stacking Faults on the Thermoelectric Figure of Merit of Si Nanowires

Kantawong Vuttivorakulchai*, Mathieu Luisier, and Andreas Schenk
Integrated Systems Laboratory
ETH Zürich
Gloriastrasse 35, CH-8092 Zürich, Switzerland
*email: kvuttivo@iis.ee.ethz.ch

***Abstract*—The efficiency of converting waste heat to electricity requires a large value of the thermoelectric figure of merit (ZT). This can be achieved by patterning bulk material into nanostructures like nanowires (NWs). Further improvement results from an increased surface roughness (SR) of such NWs [1]. In this work, Si NWs with stacking faults (SFs) are studied. It is shown that SFs can significantly reduce the lattice thermal conductivity as compared to ideal NWs [2]. A recent derivation of the phonon relaxation time for SF scattering [3] is adapted to the electronic case. It turns out that in most cases the thermoelectric power factor (PF) decreases to a lesser extent than the thermal conductivity. This can double ZT provided that SR scattering of electrons is negligible.**

Keywords—thermoelectricity, Si nanowire, stacking faults, Scattering, device modeling

I. Introduction

It has been shown experimentally that the presence of SFs strongly increases the ZT value of InAs NWs with a diameter of 20 nm [4]. To the best of our knowledge, such experiments have not been conducted yet with Si NWs, where SFs arise as the interfaces between alternating regions having either diamond (DM) or wurtzite (WZ) structure (see Fig. 1). For the first time, the simulation of such a Si NW with 70 nm in diameter will be presented.

II. Theory and Approach

First-principle calculations based on projector augmented-wave (PAW) pseudopotentials with hybrid functional of Heyd, Scuseria, and Ernzerhof (HSE06) [5] as implemented in the Vienna ab initio simulation package (VASP) were performed [6,7]. The electronic band structures are calculated for the cubic unit cells of DM oriented in ⟨100⟩ and ⟨111⟩ direction, respectively, and WZ oriented in ⟨0001⟩ direction along the x-axis. These band structures are the input for our in-house linearized Boltzmann transport equation (BTE) solver.

A. Transport Coefficients from BTE

The theoretical background of the BTE will not be outlined here as it can be found elsewhere, e.g. in Ref. [8]. The transport properties of real materials can be explained by this theory. In the presence of an electrical field (**E**) and a temperature gradient (∇T), the electrical current density $\boldsymbol{J}$ and the heat current (or energy flux density) $\boldsymbol{J}_Q$ can be written, respectively, as

$$\boldsymbol{J} = \boldsymbol{\sigma}\left(\mathbf{E} - \boldsymbol{S}\nabla\mathrm{T}\right), \tag{1}$$

$$\boldsymbol{J}_Q = \mathrm{T}\boldsymbol{\sigma}\boldsymbol{S}\mathbf{E} - \boldsymbol{K}\nabla\mathrm{T}, \tag{2}$$

where $\boldsymbol{\sigma}$, $\boldsymbol{S}$, and $\boldsymbol{K}$ are rank-two tensors which reduce to scalars for isotropic media.

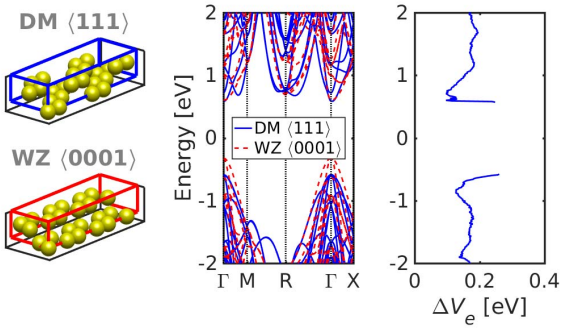

Figure 1: Left panel: Schematic view of the two (three) smallest cubic unit cells of DM (WZ) in ⟨111⟩ (⟨0001⟩) direction. Right panel: The corresponding electronic band structures calculated by density functional theory (DFT) and the energy difference between DM and WZ structures. A $\boldsymbol{k}$-point sampling of "401×101×101" is used.

The electronic part of the thermal conductivity is defined as (minus) the heat current per unit of temperature gradient in open-circuit conditions (i.e., $\boldsymbol{J} = 0$). It is given by

$$\boldsymbol{k}_e = \boldsymbol{K} - \mathrm{T}\boldsymbol{\sigma}\boldsymbol{S}^2. \tag{3}$$

By solving the BTE under relaxation time (RT) approximation and the assumption that the system is in steady state with a distribution function slightly different from its equilibrium form, the transport coefficients read

$$\left[\boldsymbol{\sigma}\right]_{ij}\left(E_F,\mathrm{T}\right) = e^2\int_{-\infty}^{\infty} dE\left(-\frac{\partial f\left(E,E_F,\mathrm{T}\right)}{\partial E}\right)\Sigma_{ij}\left(E\right), \tag{4}$$

$$\left[\boldsymbol{\sigma}\boldsymbol{S}\right]_{ij}\left(E_F,\mathrm{T}\right) = \frac{e}{\mathrm{T}}\int_{-\infty}^{\infty} dE\left(-\frac{\partial f\left(E,E_F,\mathrm{T}\right)}{\partial E}\right)\left(E-E_F\right)\Sigma_{ij}\left(E\right), \tag{5}$$

$$\left[\boldsymbol{K}\right]_{ij}\left(E_F,\mathrm{T}\right) = \frac{1}{\mathrm{T}}\int_{-\infty}^{\infty} dE\left(-\frac{\partial f\left(E,E_F,\mathrm{T}\right)}{\partial E}\right)\left(E-E_F\right)^2\Sigma_{ij}\left(E\right), \tag{6}$$

where i and j are Cartesian indices, $\partial f/\partial E$ is the derivative of the Fermi-Dirac distribution function with respect to the energy (E), E_F is the Fermi level or the electro-chemical potential, $\boldsymbol{\sigma}$, $\boldsymbol{S}$, and $\boldsymbol{k_e}$ are the electrical conductivity, Seebeck coefficient, and electron thermal conductivity, respectively. The transport distribution function (TDF) is defined as

$$\Sigma_{ij}\left(E\right) = \frac{1}{V}\sum_{n,\boldsymbol{k}} v_i\left(n,\boldsymbol{k}\right)v_j\left(n,\boldsymbol{k}\right)\tau_{n,\boldsymbol{k}}\delta\left(E-E_{n,\boldsymbol{k}}\right), \tag{7}$$

where the summation is over all bands n and the entire Brillouin zone (BZ). v_i is the i-component of the group

978-1-7281-0940-4/19/$31.00 ©2019 IEEE

velocity at $(n, \boldsymbol{k})$. The electron lifetime $\tau_{n,\boldsymbol{k}}$ is a function of both n and $\boldsymbol{k}$. The electron and hole density are given by

$$n_e\left(E_F,\mathrm{T}\right)=\int_{E_C}^{\infty} dE f\left(E,E_F,\mathrm{T}\right) DOS\left(E\right), \tag{8}$$

$$n_h\left(E_F,\mathrm{T}\right)=\int_{-\infty}^{E_V} dE\left[1-f\left(E,E_F,\mathrm{T}\right)\right] DOS\left(E\right), \tag{9}$$

respectively, where DOS is the electron density of states, E_C the conduction band edge, and E_V the valence band edge. Finally, the electron and hole mobilities are, respectively, defined as

$$\mu_e=\sigma/n_e e\,,\quad \mu_h=\sigma/n_h e\,. \tag{10}$$

The electron scattering rate is obtained by summing the inverse partial RTs of all involved scattering processes.

B. *Scattering of Electrons at Stacking Faults*

The SF scattering model developed for phonons in Ref. [3] is modified for electron scattering at SFs. The only difference is that the phonon wave function is replaced by the electron wave function ($\boldsymbol{q}$ replaced by $\boldsymbol{k}$). Only an exponential distribution of SFs is considered here. In this case the relaxation time takes the form

$$\frac{1}{\tau_{sf}(E)}=\frac{l_{sf}\Delta V^2}{\hbar^2 v_x(E)\left[1+4k_x^2 l_{sf}^2\right]}. \tag{11}$$

The average distance between SFs (l_{sf}) along the NW is assumed to be 2.5 nm. The computation of the electronic relaxation time for SF scattering requires the knowledge of the energy difference between DM in ⟨111⟩ direction and WZ in ⟨0001⟩ direction (see Fig. 1). The number of atoms must be the same in both lattice configurations, hence two (three) smallest unit cells of DM (WZ) are used. For a dense $\boldsymbol{k}$-point sampling in the BTE calculation, the first Brillouin zone is discretized by 401 points in x-direction and 101 points in the other directions.

C. *Electron-phonon Scattering on Electrons*

Apart from SF scattering, the electronic relaxation time is determined by electron-phonon scattering as shown in Fig. 2. Here, the semi-empirical treatment is used to derive the electron-phonon coupling matrix. The relaxation time approximation from the linearized BTE is defined by the relation

$$\begin{aligned}\frac{1}{\tau_{n\boldsymbol{k}}}=&\frac{2\pi}{\hbar}\sum_{mp}\int\frac{d\boldsymbol{q}}{\Omega_{BZ}}\left|g_{mnp}(\boldsymbol{k},\boldsymbol{q})\right|^2\\&\times\Big[\left(n_{qp}+f_{m\boldsymbol{k}+\boldsymbol{q}}\right)\delta\left(E_{m\boldsymbol{k}+\boldsymbol{q}}-\left(E_{n\boldsymbol{k}}+\hbar\omega_{qp}\right)\right)\\&+\left(1+n_{qp}-f_{m\boldsymbol{k}+\boldsymbol{q}}\right)\delta\left(E_{m\boldsymbol{k}+\boldsymbol{q}}-\left(E_{n\boldsymbol{k}}-\hbar\omega_{qp}\right)\right)\Big]\end{aligned}. \tag{12}$$

The right-hand side presents the modification of the distribution function arising from electron-phonon scattering in and out of the state $|n\boldsymbol{k}\rangle$, by emission or absorption of phonons with frequency $\omega_{\boldsymbol{q}p}$, and branch index p. $n_{\boldsymbol{q}p}$ is the Bose-Einstein distribution function. The matrix elements $g_{mnp}(\boldsymbol{k}, \boldsymbol{q})$ are the probability amplitude for scattering from an initial electronic state $|n\boldsymbol{k}\rangle$ into a final state $|n\boldsymbol{k}+\boldsymbol{q}\rangle$ by a phonon $|\boldsymbol{q}p\rangle$.

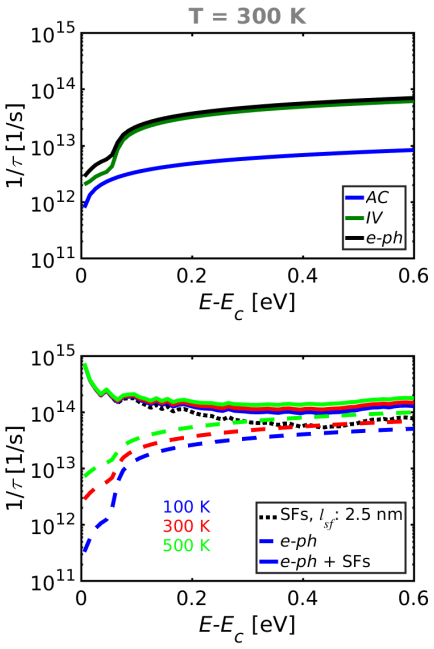

Figure 2: Energetic scattering rate of electrons from different scattering mechanisms. Top panel: The contributions of the electron-phonon (*e-ph*) scattering from acoustic phonon (*AC*) and intervalley (*IV*) scatterings at room temperature. Bottom panel: *e-ph* scattering and SF scattering with l_{sf} equal to 2.5 nm, at different temperatures. The energy zero is the conduction band edge (E_c).

The coupling of carriers with the lattice vibrations is described by the deformation potential interaction. The deformation potential involves only the short-range interaction between electrons and long-wavelength phonons. All deformation potential parameters for Si can be found in Ref. [9]. The electron-phonon coupling constants are given by the expressions

$$g_p(\boldsymbol{q})=\begin{cases}\sqrt{\dfrac{\hbar}{2\Omega\rho\omega_{pq}}}D_A|\boldsymbol{q}|, & AC\\ \sqrt{\dfrac{\hbar}{2\Omega\rho\omega_{pq}}}D_O, & OP\end{cases}, \tag{13}$$

where D_A is the acoustic (*AC*) deformation potential, D_O is the constant zero-order optical (*OP*) deformation potential and ρ is the mass density of the material. By inserting Eq. (13) into Eq. (12) with the use of a simple parabolic band model, the rates for scattering at acoustic and optical phonons, respectively, read

$$\frac{1}{\tau_{AC}}=\frac{2^{1/2}D_A^2 m_{eff}^{3/2}k_B\mathrm{T}E_{\boldsymbol{k}}^{1/2}}{\pi\hbar^4 v_{AC}}, \tag{14}$$

$$\frac{1}{\tau_{OP}}=\frac{D_O^2 m_{eff}^{3/2}}{2^{1/2}\pi\hbar^3\omega_{OP}\rho}\left[\left(n_q+\frac{1}{2}\mp\frac{1}{2}\right)\cdot\left(E_{\boldsymbol{k}}\pm\hbar\omega_{OP}\right)^{1/2}\right], \tag{15}$$

where v_{AC} is the acoustic phonon group velocity (sound velocity) and m_{eff} is the density-of-states effective mass which is equal to $(m_t^2 m_l)^{1/3}$ (m_t is the transverse effective mass and m_l is the longitudinal effective mass).

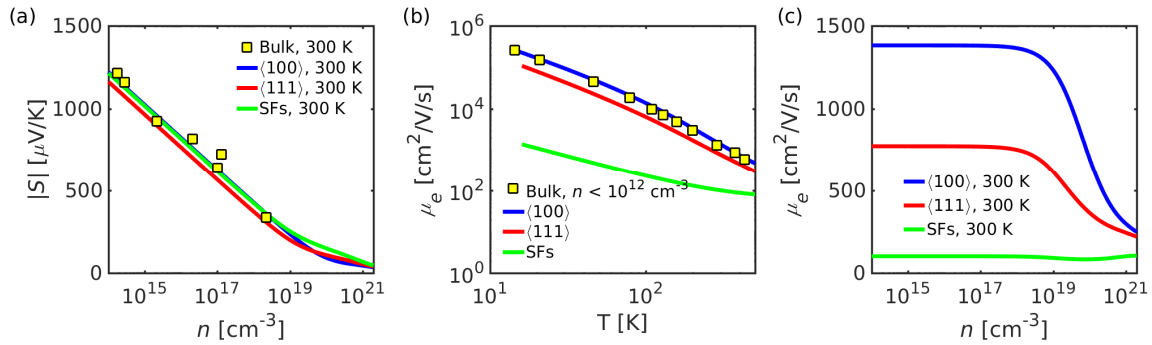

Figure 3: (a) Absolute value of Seebeck coefficient as function of electron concentration (n) at room temperature. The blue (red) line corresponds to a cubic unit cell of DM oriented in ⟨100⟩ (⟨111⟩) direction, respectively. Symbols represent the experimental data of Ref. [11]. (b) Electron mobility as function of temperature at an electron concentration of 10^{12} cm^{-3}. Symbols are experimental data from Ref. [12]. (c) Electron mobility as function of electron concentration at 300 K.

The equi-energy surfaces of Si have several valleys. Therefore, scattering between valleys (intervalley scattering) can occur. For Si, the valleys are equivalent near the zone boundary along ⟨100⟩ directions. There are two types of intervalley scattering. (i) The *g*-type processes scatter a carrier from a valley to the opposite one. (ii) The *f*-type processes scatter a carrier into one of the remaining valleys. The scattering rate of intervalley scattering can be written as

$$\frac{1}{\tau_{IV}} = \frac{D_{if}^2 m_{eff}^{3/2} Z_f}{2^{1/2}\pi\hbar^3\omega_{if}\rho}\left[\left(n_q + \frac{1}{2} \mp \frac{1}{2}\right)\cdot\left(E_k \pm \hbar\omega_{if} - \Delta E_{if}\right)^{1/2}\right]. \quad (16)$$

where D_{if} is the intervalley deformation potential which characterizes the strength of the scattering from the initial valley i to the final valley f, Z_f is the number of final valleys, ΔE_{if} is the difference between the bottom of the conduction bands in the final and the initial valleys.

SR scattering and all kinds of Coulomb scattering are ignored. The electron density is treated as a parameter. The possible impact of SR scattering would depend on the surface field that emerges as the electrostatic consequence of doping, interface charges, and fixed oxide charges. A doping level of ~1×10^{20} cm^{-3} as chosen in Ref. [10] generates flat-band conditions and makes SR scattering a second-order effect in bulk-like NWs.

III. Results

Near the conduction band edge, the energetic rate of SF scattering strongly dominates over the rate of electron-phonon scattering (Fig. 2). The latter becomes stronger when the energy increases. The figure of merit ZT is the product of PF and average temperature between two contacts, divided by the sum of lattice and electron thermal conductivities. The PF is given by the square of the Seebeck coefficient (S) multiplied by the electrical conductivity. As shown in Fig. 3(a), the calculated S of the DM structure perfectly fits the experimental data. As $|S|$ is the conductance-averaged energy difference $|E - E_F|$, it decreases with increasing density. The electron mobility of the DM structure oriented in ⟨100⟩-direction matches the measured bulk electron mobility for negligible doping concentration (< 10^{12} cm^{-3}) as can be seen in Fig. 3(b). However, the mobility of the DM structure oriented in ⟨111⟩-direction has smaller values as function of both temperature and electron concentration (see Fig. 3(c)). The structure with SFs exhibits a clear reduction of the electron mobility compared to the two DM structures.

Calculations of the lattice thermal conductivity of bulk Si and Si NWs are reproduced from Ref. [2] in Fig. 4. As in the case of InAs NWs [3], comparable reductions of the thermal conductivity of Si NWs can be obtained with SFs instead of SR. Figure 4 also presents the electronic part of the thermal conductivity as function of electron density. Its values increase with the electron concentration. When SFs are introduced into the material, the electron thermal conductivity is reduced significantly from the perfect crystal. Figure 5 shows the PF as function of electron density at 300 K and 500 K. SFs lower the PF significantly over the entire concentration range. The percentage reduction of the PF of Si NWs as the consequence of SFs reduces when the temperature increases. The ZT as function of electron concentration is presented in Fig. 5. As expected, engineering NWs increases the ZT value

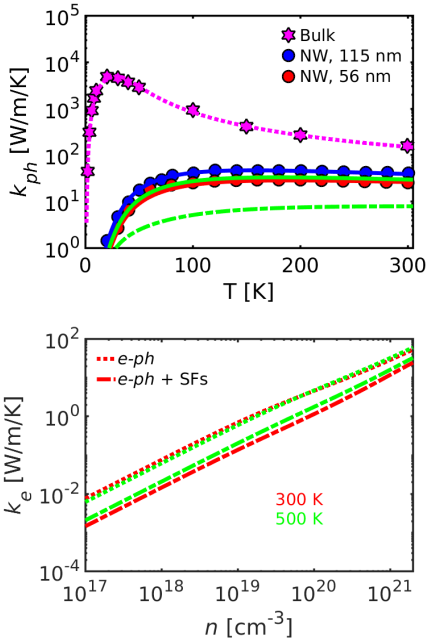

Figure 4: Top panel: Lattice thermal conductivity as function of temperature. Symbols denote the measurements from Refs. [1,13-14]. Lines are simulated thermal conductivities. The dotted line is for the bulk case, whereas solid lines are for the ideal NW case. The dash-dotted line is for a NW with SFs. Blue (green, red) lines are for 120 nm (70 nm, 56 nm) diameter, respectively. Bottom panel: Electron thermal conductivity as function of electron density with temperatures equal to 300 K and 500 K.

compared to the bulk case. The benefit of SFs to the improvement of ZT is clearly observed in the high-density range and at high temperatures. A doubling of the ZT value compared to that of an ideal NW could be achievable.

IV. Conclusion

An in-house linearized BTE solver was used to derive the ZT of bulk Si, ideal Si NWs, and Si NWs with SFs based on DFT band structure calculations for electrons and phonons. NWs with SFs have a lower electron mobility and a smaller PF. At high electron concentration, this suppression is reduced by the increasing role of electron-phonon scattering, whereas the lattice thermal conductivity remains the same. This leads to an improved ZT. Our simulations show the possibility of engineering the ZT of Si NWs by the introduction of SFs. This could encourage experimentalists to explore the benefit of such NWs for thermoelectric converters.

Acknowledgment

We acknowledge funding from the Swiss National Science Foundation through SNF under project 149454 (TORNAD).

References

[1] A. I. Hochbaum et al., "Enhanced thermoelectric performance of rough silicon nanowires," Nature, vol. 451, no. 7175, pp. 163-167, January 2008.

[2] K. Vuttivorakulchai, M. Luisier, and A. Schenk, "Effect of stacking faults and surface roughness on the thermal conductivity of Si nanowires," IWCN, pp. 23-24, May 2019.

[3] K. Vuttivorakulchai, M. Luisier, and A. Schenk, "Effect of stacking faults and surface roughness on the thermal conductivity of InAs nanowires," J. Appl. Phys., vol. 124, no. 20, pp. 205101, November 2018.

[4] P. Mensch, S. Karg, V. Schmidt, B. Gotsmann, H. Schmid, and H. Riel, "One-dimensional behavior and high thermoelectric power factor in thin indium arsenide nanowires," Appl. Phys. Lett., vol. 106, no. 9, pp. 093101, March 2015.

[5] J. Heyd, G. E. Scuseria, and M. Ernzerhof, "Hybrid functionals based on a screened Coulomb potential," J. Chem. Phys., vol. 118, no. 18, pp. 8207-8215, April 2003.

[6] G. Kresse and J. Furthmuller, "Efficient iterative schemes for ab initio total-energy calculations using a plane-wave basis set," Phys. Rev. B, vol. 54, no. 16, pp. 11169-11186, October 1996.

[7] J. P. Perdew et al., "Restoring the density-gradient expansion for exchange in solids and surfaces," Phys. Rev. Lett., vol. 100, no. 13, pp. 136406, April 2008.

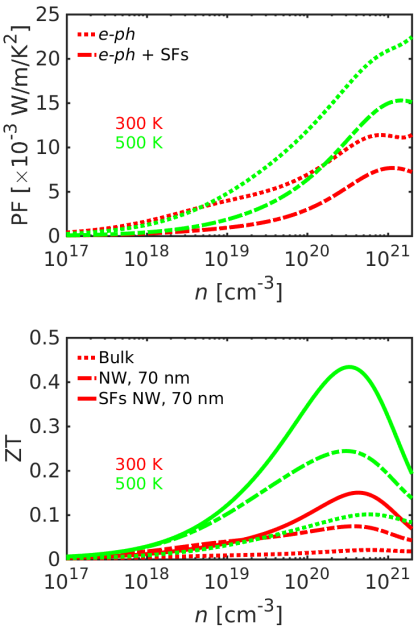

Figure 5: Top panel: Power factor as function of electron density with temperatures equal to 300 K and 500 K. Bottom panel: Thermoelectric figure of merit as function of electron density. The NW diameter is 70 nm.

[8] J. M. Ziman, "Electrons and phonons: The theory of transport phenomena in solids," ser. Oxford Classic Texts in the Physical Sciences. Oxford, New York: Oxford University Press, February 2001.

[9] C. Jacoboni and L. Reggiani, "The Monte Carlo method for the solution of charge transport in semiconductors with applications to covalent materials," Rev. Mod. Phys., vol. 55, no. 3, pp. 645-705, July 1983.

[10] A. I. Boukai et al., "Silicon nanowires as efficient thermoelectric materials," Nature, vol. 451, no. 7175, pp. 168-171, January 2008.

[11] Z. Wang et al., "Thermoelectric transport properties of silicon: Toward an ab initio approach," Phys. Rev. B, vol. 83, no. 20, pp. 205208, May 2011.

[12] C. Jacoboni, C. Canali, G. Ottaviani, and A. Alberigi Quaranta, "A review of some charge transport properties of silicon," Solid State Electron., vol. 20, no. 2, pp. 77-89, February 1977.

[13] C. J. Glassbrenner and G. A. Slack, "Thermal conductivity of silicon and germanium from 3 K to the melting point," Phys. Rev., vol. 134, no. 4A, pp. A1058-A1069, May 1964.

[14] M. G. Holland, "Analysis of lattice thermal conductivity," Phys. Rev., vol. 132, no. 6 pp. 2461-2471, December 1963.